Supplemental Material

Data S1

Tissue harvesting and blood collection

Rats were sacrificed eight days after surgery and start of treatment. Rats were fasted overnight and sacrificed at the beginning of the light cycle by isoflurane anesthesia followed by heart exsanguination. For plasma analyses, blood collected in Microvette EDTA vacutainers was supplemented with a DPPIV inhibitor; for serum analyses, blood was collected in Microvette vacutainers. After centrifugation, plasma or serum were stored at -80°C. Organs were harvested within 30 minute after exsanguination. The thoracic aorta was placed immediately in cold modified Krebs-Ringer bicarbonate solution (pH 7.4, 37°C, 95% O2, 5% CO2) of the following composition (mmol/L): NaCl (118.6), KCl (4.7), CaCl2 (2.5), KH2PO4 (1.2), MgSO4 (1.2), NaHCO3 (25.1), glucose (11.1), and calcium EDTA (0.026). The aorta was cleaned from adhering connective tissue and was either snap-frozen in liquid nitrogen and stored at -80°C or used immediately for *ex vivo* organ chamber experiments.

Dihydroethidium staining on rat aortae

Frozen 10 µm sections from aortae were cut with a Leica CM3050S cryostat and placed on positive-charged slides Superfrost Plus. Dihydroethidium (DHE) was prepared as stock solution in DMSO, diluted in deoxygenated PBS (final concentration 5 µM), and applied to frozen sections for 30 min at 37°C. Nuclei were counterstained with Hoechst 33258 (final concentration 1µg/ml). Slides were coverslipped and images taken on a SP8 microscope (10x/0.30 objective; Leica, Solms, Germany), and quantified (ImageJ, NIH). DHE fluorescence was calculated

by subtracting the auto-fluorescence signal (green channel) from the DHE signal (red channel), and normalized to the total fluorescent area.

qPCR analysis

Expression of kidney injury molecule-1 (KIM-1) and lipocalin-2 (NGAL) was analyzed by qPCR of snap-frozen kidney tissue. RNA was isolated from frozen kidneys with a RNaeasy Mini Kit and reverse transcribed with a Ready-To-Go You-Prime First-Strand Beads. Rat-specific primers were used for KIM-1 (forward: GTGGGTCACCCTGTCACAAT, reverse: ATGTTGTATCGACCGCTGCT) and NGAL (forward: GATGAACTGAAGGAGCGATTC, reverse: TCGGTGGGAACAGAGAAAAC). CT results were normalized to GAPDH CT.

Histological analysis

Representative samples of aorta, liver, pancreas, kidneys, thyroid glands, inguinal white adipose tissue and interscapular brown adipose tissue were fixed in 10% neutral buffered formalin and embedded in paraffin. Sections (3-5 µm) were prepared, mounted on glass slides, deparaffinised in xylene, rehydrated through graded alcohols and stained with haematoxylin and eosin (H&E) for the histological examination. All slides were scanned using digital slide scanner NanoZoomer-XR C12000 (Hamamatsu, Hamamatsu City, Japan) and images were taken using NDP-view2 viewing software (Hamamatsu).

Renal injury, characterized by tubular degeneration and regeneration and interstitial inflammation, was assessed by light microscopy in a blinded fashion (by G.P.). A semi-quantitative scoring of 0-5 was employed, based on the proportion of affected tubules: 0, none; 1, <10% (slight injury); 2, 11-25% (mild); 3, 26-45% (moderate); 4, 46-75% (marked); and 5, >75% (severe).

Supplemental Results

JNK2 inhibition after *in vivo* SP600125 treatment induces protective vascular effects similar to RYGB

In the pilot experiment, eight-day treatment of DIO sham-operated *ad libitum*-fed rats with SP600125 increased endothelium-mediated relaxation in response to GLP-1 and insulin similar to RYGB, although the effect was less pronounced than in RYGB rats (Fig. S1E-F). *In vivo* SP600125 treatment decreased aortic JNK2 phosphorylation compared to controls$_{DMSO}$ rats, while JNK1 phosphorylation was not affected (Fig. S2A). JNK2 inhibition was followed by decreased IRS-1 Ser307 and increased Akt Ser473 phosphorylation and higher eNOS dimerization similar to RYGB and D-JNK treatment (Fig. S2B-E). Additionally, *in vivo* SP600125 treatment also decreased aortic superoxide anion levels and NADPH activity comparable to RYGB surgery (Fig. S5A-B). SP600125 did not affect circulating GLP-1 levels (Fig. S5C). These results support a direct role of vascular JNK2 inactivation in lowering oxidative stress and activating Akt/eNOS signaling pathways to improve endothelial function after RYGB, and prompted us to perform the main experiment using the more specific JNK inhibitor D-JNK.

Aortic eNOS Ser116 phosphorylation

It has been published that JNK2 directly inhibits eNOS by Ser116 phosphorylation in studies using bovine aortic endothelial cells [1] and mouse aortae [2]. Unfortunately, we could not detect eNOS Ser116 phosphorylation in rat aorta with the same anti-human Ser116 antibody used in previous publications [1, 2]. This antibody, which is the only commercially available anti-phospho-Ser 116 eNOS, showed bands between 100 kDa and 130 kDa, but not at 140 kDa, which is the expected molecular

weight of eNOS. In contrast, total eNOS was detected at 140 kDa (Fig. S3). The eNOS Ser116 antibody has not been validated in rat tissue before (personal communication; Merck Millipore) and the only available results had been obtained with bovine aortic endothelial cells [1]. One study assessed eNOS Ser116 in mice aortae, but representative images for total and phosphorylated eNOS did not report the molecular weight references to rule out an unspecific binding [2]. A sequence alignment of the human and rat immunogenic regions used for this antibody showed sub-optimal homology, suggesting limited reactivity (personal communication; Merck Millipore). Therefore, it is possible that the antibody is not suitable to detect eNOS Ser116 phosphorylation specifically in rat tissue.

D-TAT carrier peptide-dependent kidney toxicity

D-JNK treatment affected food intake and body weight similar to RYGB (Fig.6B-C), while SP600125 or D-JNK in chow-fed lean rats (Fig. S6A-C) had no effect. This prompted us to investigate organ toxicity as a potential cause of weight loss after chronic D-JNK treatment in obese rats. Circulating markers of liver and kidney damage were assessed (urea, creatinine, cystatin C, transferrin, albumin, alanine aminotransferase, aspartate aminotransferase, lactate dehydrogenase). Only creatinine and cystatin C levels were significantly elevated in the D-JNK group, suggesting potential kidney toxicity (Fig. S6D-E). Furthermore, histological analysis indicated tubular degeneration and necrosis, accompanied by tubular regeneration and interstitial, predominantly lymphohistiocytic cell infiltration (Fig. S7A-B). Renal injury also occurred in controls$_{D\text{-}TAT}$ rats but was more moderate (approximately 40% tubules affected) compared to D-JNK-treated rats (> 80%). These histological changes were accompanied by impaired kidney function in

controls$_{D\text{-}TAT}$ and D-JNK animals, with increased urinary excretion and a presumably compensatory higher water intake (Fig. S7C-F). There was no statistically significant difference in urine excretion and water intake between controls$_{D\text{-}TAT}$ and D-JNK animals. Gene expression analysis of acute kidney injury markers showed increased kidney injury molecule-1 (KIM-1) and neutrophil gelatinase-associated lipocalin/lipocalin 2 (NGAL) in obese rats upon D-JNK and D-TAT treatment (Fig. S7G-H). A slight increase of these kidney injury markers was also observed in chow-fed D-TAT- and D-JNK-treated animals while SP600125 did not affect KIM-1 and NGAL expression (Fig. S7G-H). The analyses of aorta, liver, pancreas, thyroid glands, white and brown adipose tissue from controls$_{D\text{-}TAT}$ and D-JNK rats did not show biochemical or histological signs of toxicity (data not shown), suggesting a kidney-specific effect. To our knowledge, this is the first study clearly showing *in vivo* D-JNK toxicity in the kidney. Published data on D-JNK pharmacokinetics after a single intra-peritoneal injection in mice reported a higher accumulation of D-JNK in the filter organs (kidney and liver) and in urine for up to one week, suggesting that D-JNK excretion is almost exclusively urinary [3]. In D-JNK, the active JNK inhibitory peptide is conjugated to a commonly used cell-penetrating oligo-peptide, the HIV-1 TAT protein, which functions as a carrier [4]. It has been reported that various cell-permeable peptides, including D-TAT oligo-peptides such as D-JNK, induce *in vitro* length-dependent cytotoxic effects irrespective of their sequence [5]. Therefore, the observed kidney damage was likely due to intrinsic cytotoxicity of the D-TAT carrier peptide independent of the D-JNK inhibitory activity [5]. This would explain why renal toxicity, which was observed in both controls$_{D\text{-}TAT}$ and D-JNK rats, was more pronounced in the D-JNK rats because of the peptide length. No toxicity was observed with SP600125, which supports the independence of toxicity from the JNK inhibitory activity of D-JNK.

Supplemental Figures

Figure S1

Concentration–response curves after 30 minute pre-incubation with 10^{-4} mol/L endothelial NO synthase inhibitor, L-NAME and submaximal contraction to NE in response to **(A)** GLP-1 and **(B)** insulin in $controls_{D\text{-}TAT}$, RYGB, and D-JNK rats (n=3 per group). Concentration–response curves after submaximal contraction to NE in response to **(C)** GLP-1 and **(D)** insulin in non-operated, chow-fed rats treated with D-TAT or D-JNK for eight days (n=2-4 per group). Relaxations in response to **(E)** GLP-1 and **(F)** insulin in RYGB, $controls_{DMSO}$, and SP600125 rats (*, **, *** p<0.05, p<0.01, p<0.001 RYGB vs. $controls_{DMSO}$, $^{\&\&, \&\&\&}$ p<0.01, p<0.001 RYGB vs. SP600125, as determined by two-way repeated measures ANOVA and Bonferroni post hoc test; n=5-10 per group). Results are shown as mean ± SD.

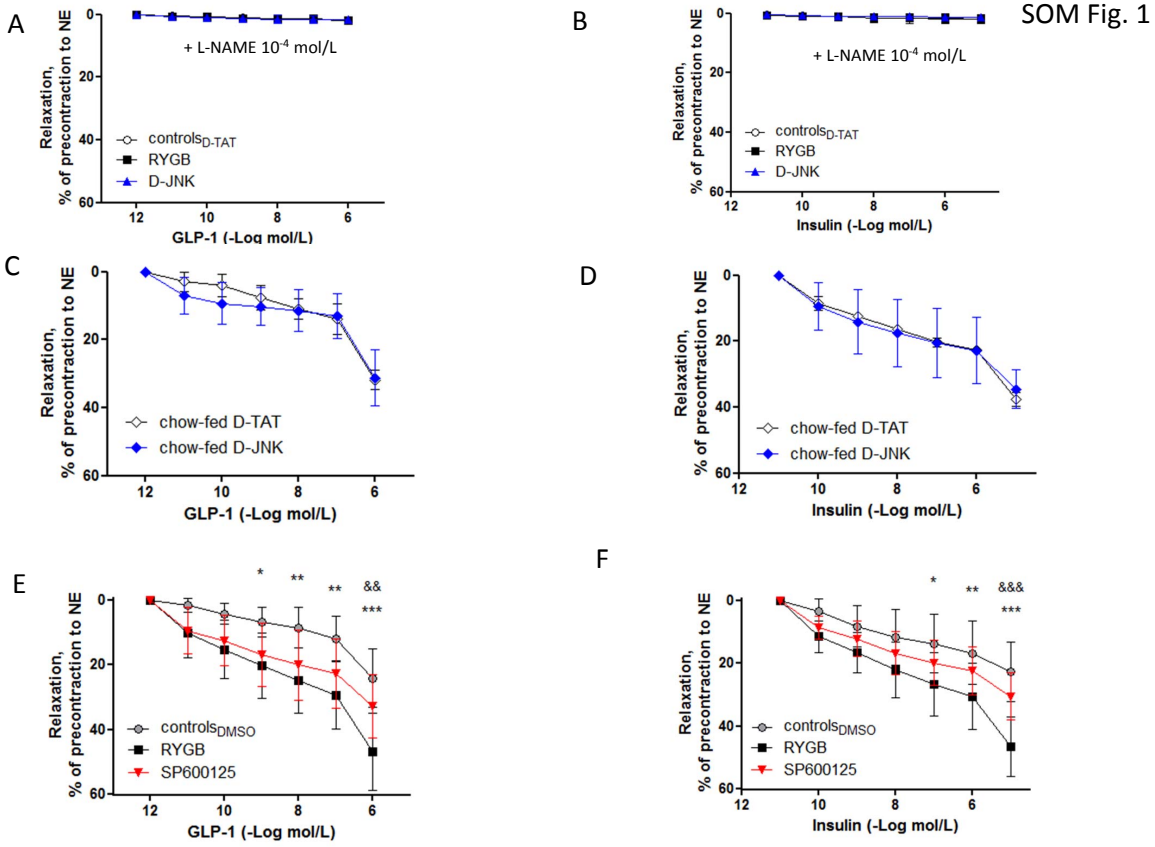

SOM Fig. 1

Figure S2

Aortic **(A)** JNK1 and JNK2 phosphorylation, **(B)** IRS-1 Ser307, **(C)** Akt Ser473, **(D)** eNOS Ser1177 phosphorylation and **(E)** eNOS dimerization in $controls_{DMSO}$, RYGB, and SP600125 rats eight days after surgery/start of treatment. Representative Western blots and densitometric quantifications are shown (*, **, *** p<0.05, p<0.01, p<0.001 RYGB vs. $controls_{DMSO}$, §, §§ p<0.05, p<0.01 $controls_{DMSO}$ vs. SP600125, as determined by one-way ANOVA and Bonferroni *post hoc* test; n=5-11 per group). Results are shown as mean ± SD.

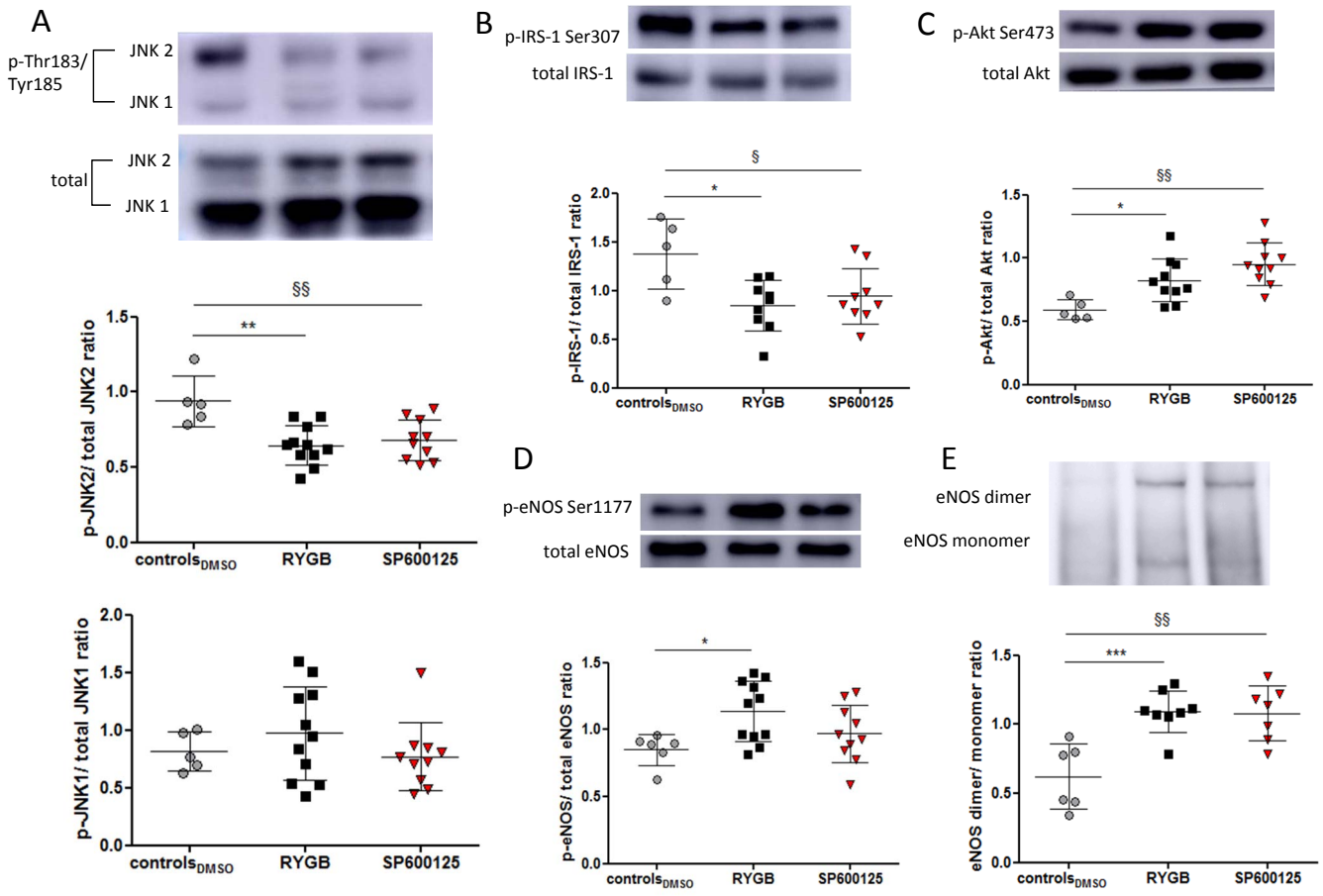

SOM Fig. 2

Figure S3

Western blot analysis of **(A)** eNOS Ser116 phosphorylation and **(B)** total eNOS (molecular weight of 140 kDa) in the same aortic lysates from controls$_{D\text{-}TAT}$, RYGB, and D-JNK rats. Representative pictures are shown.

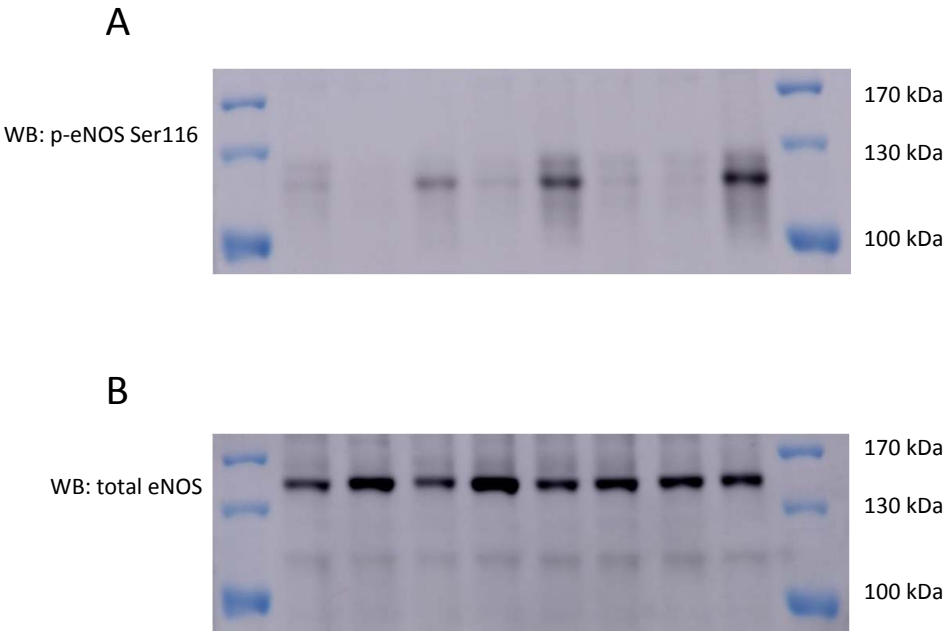

SOM Fig. 3

Figure S4

Western blot analysis of phosphorylation of **(A)** PKC alpha/beta Thr638/641, **(B)** PKCβII Ser 660, **(C)** PKCδ Thr 505, **(D)** p38 MAPK Thr180/Tyr182, **(E)** ERK1/2 (44 and 42 KD, respectively) in $controls_{D\text{-}TAT}$, RYGB, and D-JNK rats eight days after surgery/start of treatment. Representative Western blots and densitometric quantifications are shown (* $p<0.05$ D-JNK vs RYGB and $controls_{D\text{-}TAT}$, as determined by one-way ANOVA and Bonferroni post hoc test; n=7 per group). Results are shown as mean ± SD.

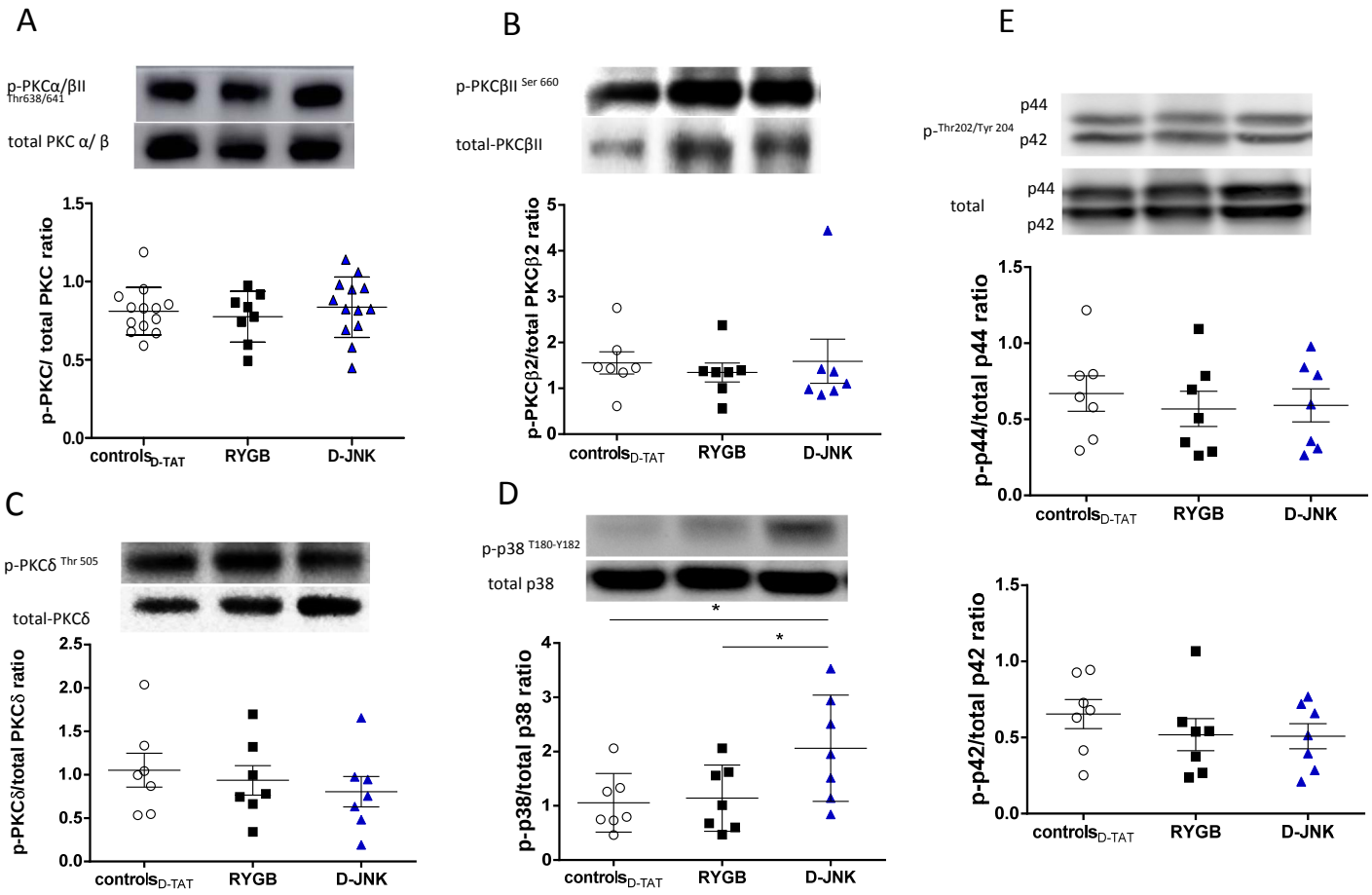

SOM Fig. 4

Figure S5

(A) *In vitro* DHE fluorescent staining of anion superoxide and relative quantification in aortae isolated from $controls_{DMSO}$, RYGB and SP600125 rats eight days after surgery/start of treatment. Representative pictures are shown. **(B)** *In vitro* NADPH oxidase activity in aortae isolated eight days after surgery (* $p<0.05$ RYGB vs. all other groups, § $p<0.05$ $controls_{DMSO}$ vs. SP600125, as determined by one-way ANOVA and Bonferroni *post hoc* test; n=7-9 per group)**. (C)** Fasting plasma GLP-1 levels (* $p<0.05$ RYGB vs. all other groups, as determined by Kruskal-Wallis test and Dunn's Multiple Comparison test; n=6-16 per group). Results are shown as mean ± SD except in Figure S5C where results are presented as median ± IQR.

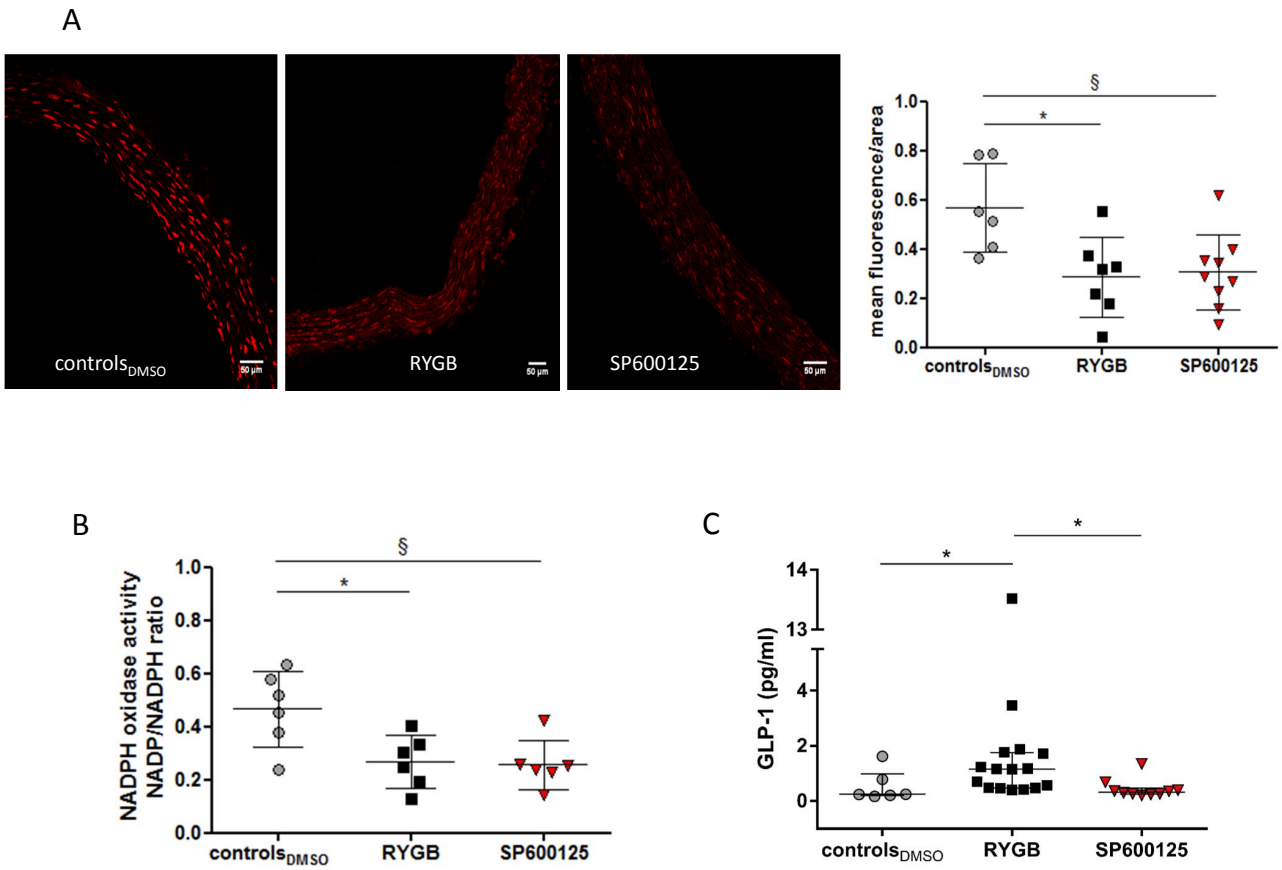

SOM Fig. 5

Figure S6

(A) Cumulative 24-hour food intake (*, **, *** p<0.05, p<0.01, p<0.001 RYGB vs. $controls_{D\text{-}TAT}$, $controls_{DMSO}$, as determined by two-way ANOVA and Bonferroni *post hoc* test; n=8-13 per group) and **(B)** body weight of $controls_{DMSO}$, RYGB and SP600125 rats before and after surgery and start of treatment (day 0) (*, ** p<0.05, p<0.01 RYGB vs. $controls_{D\text{-}TAT}$, $controls_{DMSO}$, as determined by two-way repeated measures ANOVA and Bonferroni *post hoc* test; n=8-13 per group). **(C)** Body weight (n=4 per group) in non-operated, chow-fed rats treated with D-TAT or D-JNK for eight days (no differences, as determined by two-way repeated measures ANOVA and Bonferroni *post hoc* test; n=2-4 per group). **(D)** Serum creatinine and **(E)** plasma cystatin C levels in $controls_{D\text{-}TAT,}$ RYGB, and D-JNK rats eight days after surgery/start of treatment (** p<0.01 RYGB vs. D-JNK, ° p<0.05 controlsD-TAT vs. D-JNK, as determined by Kruskal-Wallis test and Dunn's Multiple Comparison test; n=6-8 per group). Results are shown as mean ± SD except in Figure S6D-E where results are presented as median ± IQR.

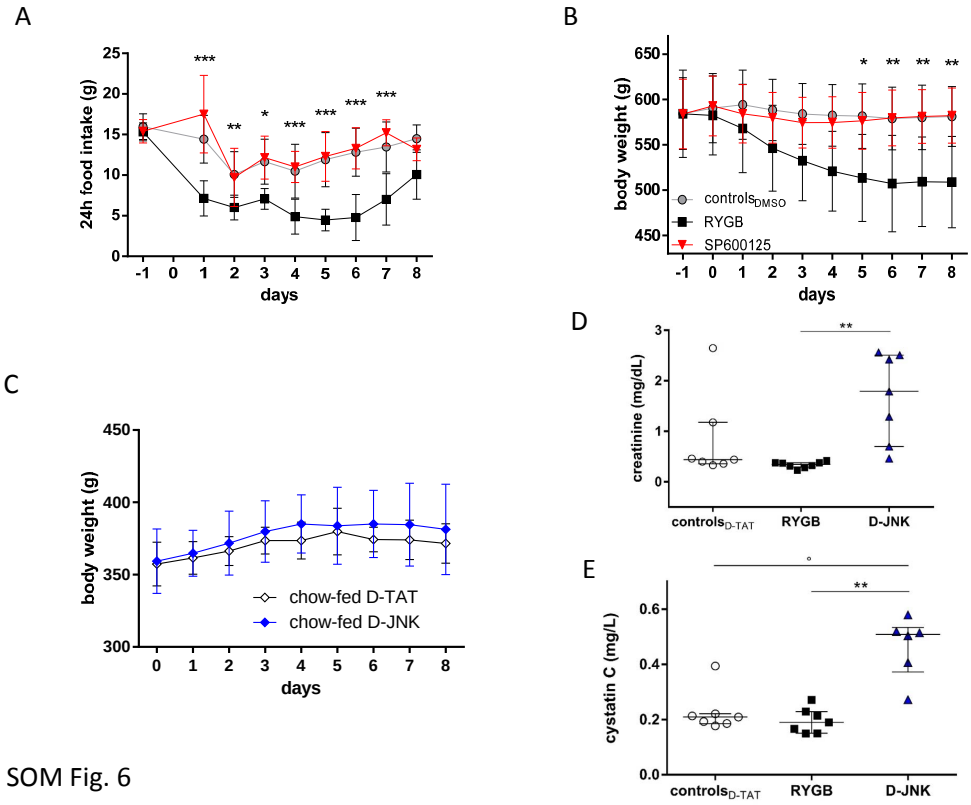

SOM Fig. 6

Figure S7

Histological analysis by hematoxylin and eosin (H&E) staining of kidney from **(A)** a D-JNK and **(B)** a $controls_{D\text{-}TAT}$ rat euthanized eight days after sham surgery/start of treatment. Cumulative 24-hour urine excretion in **(C)** $controls_{D\text{-}TAT}$ rats and **(D)** D-JNK rats, and cumulative 24-hour water intake in **(E)** $controls_{D\text{-}TAT}$ rats and **(F)** D-JNK rats 1 day before and 7 and 8 days after surgery and start of treatment (#, ##, ### $p<0.05$, $p<0.01$, $p<0.001$ Day -1 vs. Day 7 and Day 8, as determined by one-way ANOVA and Bonferroni *post hoc* test; n=6 per group). qPCR analysis of kidney expression of **(G)** kidney injury molecule-1(KIM-1) and **(H)** neutrophil gelatinase-associated lipocalin (NGAL) eight days after surgery and start of treatment (°, °°° $p<0.05$, $p<0.001$ D-JNK vs. all other groups, as determined by Kruskal-Wallis test and Dunn's Multiple Comparison test; n=4-7 per group). Results are shown as mean ± SD except in Figure S7G-H where results are presented as median ± IQR.

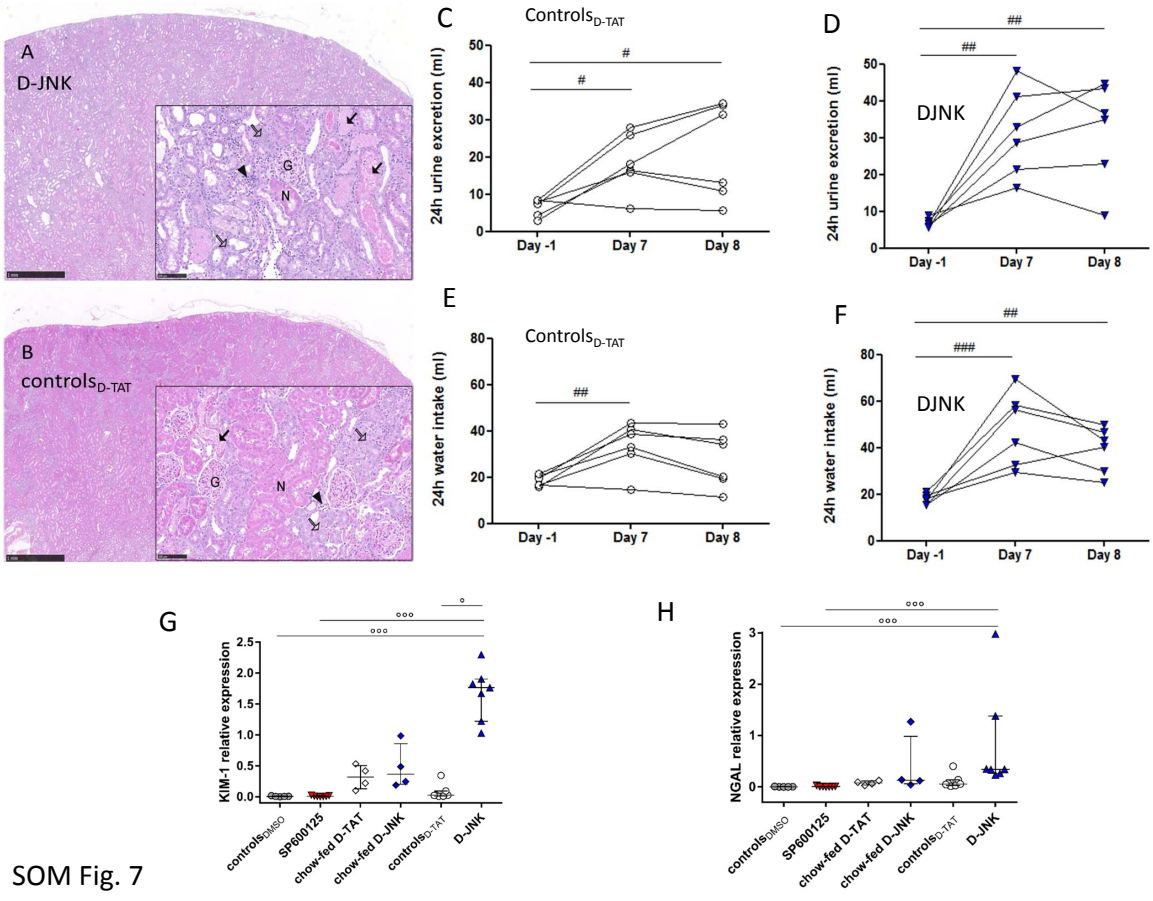

SOM Fig. 7

Supplemental References

1. Park JH, Park M, Byun CJ, Jo I. C-jun n-terminal kinase 2 phosphorylates endothelial nitric oxide synthase at serine 116 and regulates nitric oxide production. *Biochemical and biophysical research communications*. 2012;417:340-345
2. Cho DH, Park JH, Joo Lee E, Jong Won K, Lee SH, Kim YH, Hwang S, Ja Kwon K, Young Shin C, Song KH, Jo I, Han SH. Valproic acid increases no production via the sh-ptp1-cdk5-enos-ser(116) signaling cascade in endothelial cells and mice. *Free radical biology & medicine*. 2014;76:96-106
3. Davoli E, Sclip A, Cecchi M, Cimini S, Carra A, Salmona M, Borsello T. Determination of tissue levels of a neuroprotectant drug: The cell permeable jnk inhibitor peptide. *Journal of pharmacological and toxicological methods*. 2014;70:55-61
4. Bonny C, Oberson A, Negri S, Sauser C, Schorderet DF. Cell-permeable peptide inhibitors of jnk: Novel blockers of beta-cell death. *Diabetes*. 2001;50:77-82
5. Cardozo AK, Buchillier V, Mathieu M, Chen J, Ortis F, Ladriere L, Allaman-Pillet N, Poirot O, Kellenberger S, Beckmann JS, Eizirik DL, Bonny C, Maurer F. Cell-permeable peptides induce dose- and length-dependent cytotoxic effects. *Biochimica et biophysica acta*. 2007;1768:2222-2234